ACS OMEGA

Open Access

http://pubs.acs.org/journal/acsodf

Article

Dynamic-Covalent Mesoporous Silica Nanohybrid with pH/ROS-Responsive Drug Release for Targeted Tumor Therapy

Yurong Leng, Yanmei Wu, Wenjing Xiao, Xiaoquan Su, and Zhe Liu*

Cite This: *ACS Omega* 2024, 9, 47428−47435

Read Online

ACCESS | Metrics & More | Article Recommendations | Supporting Information

ABSTRACT: Nanomedicine provides promising new methodologies for the treatment of tumors but still faces several limitations, including poor colloidal stability, uncontrollable drug release, and insufficient drug targeting. Herein, hyaluronic acid (HA) was used to modify the surface of mesoporous silica nanoparticles (MSNs) via a dynamic-covalent linker, phenylborate ester (PBAE), termed MA. The HA modifier provided enhanced colloidal stability to the hybrid nanoparticles. As expected, MA exhibited an improved biocompatibility and high potential for biomedical applications. Moreover, MA with a negatively charged surface effectively adsorbed the drug Doxorubicin (DOX) inside the carriers, ensuring minimal drug leakage. In an acidic and reactive oxygen species (ROS)-containing condition mimicking the tumor microenvironment, MA@DOX (MAD) continuously released its payloads, likely due to the cleavage of the pH/ROS-sensitive PBAE. Compared with free DOX, MAD had 2.2 times higher accessibility to tumor cells than free DOX. The favorable stability and cancer-selective drug release make this nanoformulation a promising platform for potent cancer treatment.

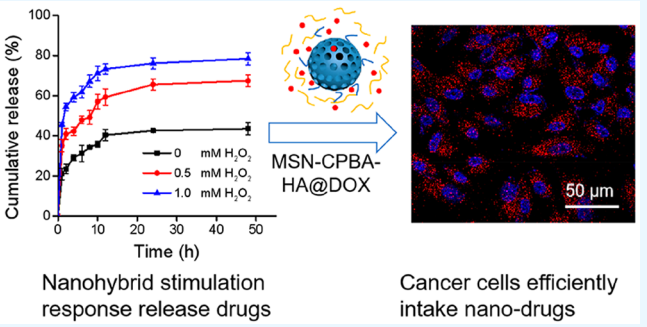

1. INTRODUCTION

The advances in nanotechnology revolutionize the drug delivery in cancer therapy.[1,2] Due to the unique particle size (ranging from 5 to 200 nm), nanosized formulations preferentially accumulate in tumors through the enhanced permeability and retention effect.[3] Inspired by this, a myriad of nanocarriers have emerged for loading various chemotherapeutic agents.[4,5] These nanodrugs aim to provide optimized therapy with high activity and minimal toxicity.[6] However, clinical outcomes have been far from anticipated. The suboptimal efficiency results from several shortcomings of drug delivery nanosystems, including limited stability in blood and poor targeting efficiency of therapeutics.[7] Stability is an essential property of any effective drug delivery vehicle.[8] Unfortunately, colloidal particle-based vehicles are prone to forming aggregates during storage and blood circulation due to their large specific surface area.[9] These aggregates not only increase the likelihood of uptake by macrophages but also pose threats to healthy tissues.[10] Additionally, targeting ability largely determines the successful use of nanocarriers.[11] A desired targeting property enables nanodrugs to reach the tumor site actively and release their payloads in response to the specific tumor environment.[12] On the opposite side, nanocarriers with poor targeting fail to elicit effective therapeutic responses and may also cause severe side effects.[13] Therefore, it is imperative to develop advanced drug delivery systems with sufficient stability and targeting to facilitate cancer therapy.

In the past decade, nanohybrids with tailored properties have attracted significant attention for developing advanced drug carriers.[14] Nanohybrids consist of inorganic components, including gold nanoparticles,[15] iron oxide nanoparticles,[16] and mesoporous silica nanoparticles (MSNs),[17] as well as organic components[18] such as polymers and biomacromolecules.[19] MSN possesses many advantages, which include a facile synthesis method, tailorable textural parameters, and a porous architecture, which make them suitable for drug delivery.[20] Despite their notable performance, relatively weak stability and low bioactivity hinder their further application in clinical settings.[21] To address these problems, the surfaces of MSNs are commonly modified with various organic agents, such as hyaluronic acid (HA),[22] chitosan,[23] gelatin,[24] and polydopamine.[25] Among these materials, HA has gained significant popularity as a candidate for functionalizing MSN.[26] In addition to stabilizing nanoparticles in the blood, HA enables MSNs to bind directly with CD44-overexpressing cancer cells.[27] However, inefficient drug release remains a major challenge for HA-modified MSNs.[28] The effectiveness of HA-

Received: May 12, 2024
Revised: October 27, 2024
Accepted: November 7, 2024
Published: November 18, 2024

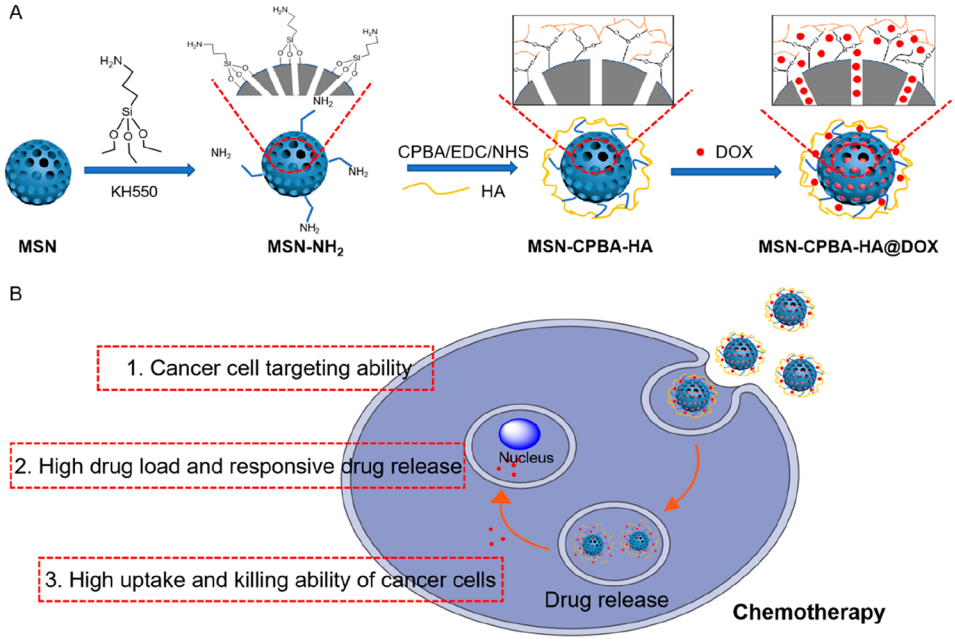

Figure 1. Schematic illustration of the (A) development of dynamic-covalent mesoporous silica nanohybrids and (B) their advantages for precise drug delivery.

modified MSN nanomedicine in achieving sustained drug release in response to tumor stimulation is found to be limited when faced with the complex tumor microenvironment.[29]

To achieve optimal efficiency in therapeutic medicines, nanocarriers must site-selectively release their payloads at precise concentrations upon reaching the lesion area. This can be achieved by introducing environmental stimuli responsiveness.[30] Solid tumors are characterized by weak acidity,[31] high levels of reactive oxygen species (ROS),[32] increased amounts of glutathione (GSH),[33] hypoxia, and overexpressed enzymes,[34] which offer various signals for constructing smart and responsive drug delivery systems.[35] Compared to other systems, ROS-responsive systems provide higher selectivity due to the sharp contrast of ROS levels between tumor tissue and normal tissue.[36] The functionality of ROS-responsive nanocarriers relies on the use of certain moieties that disassemble in the presence of elevated ROS concentrations.[37] Many functional groups have been utilized in the fabrication of ROS-responsive platforms, such as diselenide bonds, boronic ester bonds, poly(sulfide) bonds, poly(thioketal) bonds, etc.[38] Notably, boronic esters belong to dynamic covalent chemical bonds, with binding affinity sensitive to the surrounding environment. For instance, boronic esters readily cleave into boric acid and diols upon exposure to 100 mM H_2O_2.[39] Furthermore, the binding affinity of boric acid to diols is pH-responsive, with the borate structure dissociating when the pH of the environment drops below the pK_a value of boric acid. Consequently, the distinctive properties of boric acid are highly significant in the development of pH-responsive nanomedicines.[40,41] Thus, the superior sensitivity to ROS and pH sensitivity make boronic esters and their derivatives valuable components in the development of controlled carriers.

Herein, we propose a novel hybrid nanocarrier with the desired colloidal stability. The nanohybrids enabled the distinction of neoplastic cells from normal ones and allowed for the controllable release of antitumor drugs. The borate cross-linking of HA enables the formation of a stable and biocompatible shell structure, which encapsulates the therapeutic agents within. This shell structure further enhances the targeting specificity toward tumor cells that exhibit an elevated expression of CD44 receptors (Figure 1). The MSNs were selected as building blocks for constructing this advanced drug delivery system. To enhance the targeting ability and stability of MSNs, HA was used to modify MSNs through a dual-responsive linkage, phenylborate ester (PBAE). During the synthesis process, bare MSNs were first amino-functionalized and then reacted with carboxyphenylboronic acid (CPBA) via an amide reaction. Subsequently, MSNs-CPBA allowed for the grafting of 1,2-diol-containing HA, which created the dynamic-covalent PBAE. The presence of exterior HA not only stabilized MSNs but also imparted a targeting ability to the nanocarriers. Moreover, these nanocarriers possessed accelerated drug release in response to a weakly acidic pH and high levels of ROS, which further enhanced drug availability. Therefore, the rational design of this hybrid nanocarrier system offers enhanced colloidal stability, targeted drug release, and improved antitumor efficacy. This innovative approach holds great potential for future applications in cancer therapeutics.

2. MATERIALS AND METHODS

2.1. Materials. 1-(3-(Dimethylamino)-propyl)-3-ethylcarbodiimide hydrochloride (EDC·HCl), *N*-hydroxysuccinimide (NHS), hexadecyltrimethylammonium bromide (CTAB), tetraethyl orthosilicate (TEOS), and 3-aminopropyltriethoxysilane (APTES) were purchased from Sinopharm Chemical Reagent Co., Ltd. (Shanghai, China). Doxorubicin (DOX) was obtained from Dalian Meilun Biotechnology Co., Ltd. (Dalian, China). HA (MW 50 kDa) was purchased from Freda Biochem Co., Ltd. (Shandong, China). Dimethyl sulfoxide (DMSO) and CPBA were obtained from Aladdin Chemical Reagent Co., Ltd. (Shanghai, China). Dulbecco modified Eagle medium (DMEM) was purchased from Solarbio Science & Technology Co., Ltd. (Beijing, China). Fetal bovine serum

https://doi.org/10.1021/acsomega.4c04502
ACS Omega 2024, 9, 47428−47435

(FBS) was supplied by Viva Cell Biosciences Co., Ltd. (Shanghai, China).

2.2. Preparation of MSN-NH_2. MSN was synthesized by the sol−gel method.[42] In brief, 1 g of CTAB was dissolved in 480 mL of ultrapure water, followed by the addition of 280 mg of sodium hydroxide, and the mixture was then heated to 75 °C under stirring. Thereafter, 5.8 mL of TEOS was slowly added to the CTAB solution, and the mixture was allowed to react for 4 h. The resulting nanoparticles were collected after centrifugation and washed three times with ultrapure water and ethanol. Subsequently, the preprepared nanoparticles were refluxed with 500 mL of ethanol containing 6 mL of hydrochloric acid for 24 h to remove the CTAB. After centrifugation, the nanoparticles were further refluxed for 24 h in the mixture of 1 mL APTES and anhydrous toluene, resulting in the formulation of MSN-NH_2.

2.3. Preparation of MA Nanoparticles. 0.15 g portion of CPBA was mixed with 0.10 g of NHS and 0.20 g of EDC in 5 mL of stirred DMSO. Meanwhile, 400 mg of MSN-NH_2 was dispersed in 20 mL of DMSO and then added to the above solution. After reaction for 24 h, the mixture was subjected to centrifugation, and the obtained products (MSN-CPBA) were washed three times with ultrapure water and methanol.[43] Subsequently, HA was dissolved in ultrapure water, followed by the addition of MSN-CPBA, and stirred for 3 h. The resulting solution was washed three times with ethanol and ultrapure water and then lyophilized to obtain MSN-NH_2−CPBA-HA (MA) nanoparticles.[27]

2.4. Loading of DOX. Ten mL portion of MA nanoparticle solution (5 mg/mL) was mixed with 1 mL of DOX aqueous solution (2 mg/mL). After overnight stirring, the mixture was subjected to dialysis using a dialysis bag (MW: 8000−14,000) to obtain MA@DOX (MAD). The dialysate was collected, and its absorbance was measured using a UV−vis spectrophotometer (UV-3600).[44] The formula applied to analyze the encapsulation efficiency (EE %) of DOX was as follows:

$$\mathrm{EE\%} = \frac{W_T - W_D}{W_T} \times 100\%$$

where W_T is the total content of the used DOX initially, and W_D is the amount remaining in dialysate.

2.5. Characterization. The morphology of MSN and MAD was examined using transmission electron microscopy (TEM, JEM-210003040700, Japan). The hydrodynamic diameter and surface charge of the prepared nanoparticles were analyzed by using dynamic light scattering (DLS; Nano ZS 90, Malvern). The pore size and specific surface area of all the nanoparticles were measured by an automated surface area and porosity analyzer (BET, Autosorb IQ, Quantachrome, USA). The microstructure of different samples was analyzed using a Fourier infrared spectrometer (FTIR, Nicolet is50). Thermal properties and crystallinity were analyzed in thermogravimetry analysis (TGA2, Mettler Toledo, Switzerland).

2.6. Drug Release Study. For drug release studies, 1 mg/mL of MAD sample was placed into a dialysis bag, and the dialysis bag was put into 30 mL of PBS solution with different pHs (5.0, 6.5, and 7.4). Then, at different time intervals, the periodically aspirated PBS solution (3 mL) was subjected to the UV−vis detection at 280 nm.[45] In the whole process, the overall volume of dialysate was unchanged by supplementing fresh PBS. The DOX release profiles were also studied in the absence or presence of H_2O_2 (0.5 and 1.0 mM) according to the method mentioned above.[46]

2.7. In Vitro Cytotoxicity. L929 fibroblast cells (L929) were employed to evaluate the biocompatibility of prepared nanocarriers using standard CCK-8 assays.[47] Briefly, L929 cells were incubated in the T25 culture flasks containing DMEM medium and 10% (v/v) FBS. Upon reaching 80% confluence, L929 cells were collected and transferred to 96-well plates at a density of 1×10^5 cells/well. After incubation for 24 h, the medium was refreshed and added additional PBS, MSN, and MA with different concentrations (25, 50, 100, 200, and 400 μg/mL), followed by incubation for further 48 h. Then, the optical density values at 520 nm were measured using a microplate reader to calculate the cell viability using the following equation.

$$\mathrm{Cellviability(\%)} = \frac{\mathrm{OD_{samples}} - \mathrm{OD_{blanks}}}{\mathrm{OD_{Control}} - \mathrm{OD_{blanks}}} \times 100\%$$

where OD_{blanks}, $OD_{control}$, and $OD_{samples}$ were the optical density values for the blank groups, control groups, and experimental groups, respectively.

2.8. In Vitro Cellular Uptake. The cellular uptake behavior of MAD was evaluated using the cell counting kit-8 (CCK-8) method.[48] Briefly, the human lung adenocarcinoma cell line (A549) at a density of 1×10^6 was cultivated in 6 mm confocal dishes for 24 h. Then, A549 cells were treated with either MAD or free DOX (equivalent to 2 μM of DOX) for 4 and 24 h. At the predetermined time points, the cells were collected and fixed, followed by staining with DAPI. After washing three times, the cells were observed under a confocal fluorescence microscope (CLSM, Nikon A1SiR, Japan).

2.9. Statistical Analysis. All results are presented as the mean ± standard deviation (SD). For direct comparison between the two groups, the unpaired Student's t test was used. *$P < 0.05$; **$P < 0.01$; ***$P < 0.001$; n.s., not significant ($P > 0.05$).

3. RESULTS AND DISCUSSION

3.1. Fabrication and Physiochemical Characterization of MAD Nanoparticles. Several nanoscale carriers have been approved for clinical therapy or clinical trials, such as lipids, dendrimers, gold nanoparticles, and MSNs.[49] Among them, MSNs are a type of material with a highly ordered pore structure, with pore sizes ranging from 2 to 50 nm. This unique structure endows MSNs with high surface area, large pore volume, and tunable pore sizes, making them excellent candidates for drug delivery systems.[31] In this study, TEOS was used as a precursor in sol−gel chemistry to produce silica nanoparticles. After the bare MSNs were synthesized, amino groups (−NH_2) were grafted onto the surface of the MSNs and then reacted with cyclohexyl-phenyl-boronic acid (CPBA), which contains boronic acid groups (−BOH). The presence of −BOH on the surface of MSN allowed for dynamic complexation with the hydroxyl groups (−OH) of HA, thus forming HA-modified MSNs via the generation of borate bonds. As shown in Figure 2A, the spherical shape of MSNs exhibited clear mesoporous channels as visualized by TEM. When HA was grafted onto the MSN, an obvious polymer layer was formed, while the elemental mapping analysis confirmed that HA was evenly distributed on the surface of the MSN (Figure 2B,C). The formation of aggregates is a result of the unique shell structure formed by HA on the

https://doi.org/10.1021/acsomega.4c04502
ACS Omega 2024, 9, 47428−47435

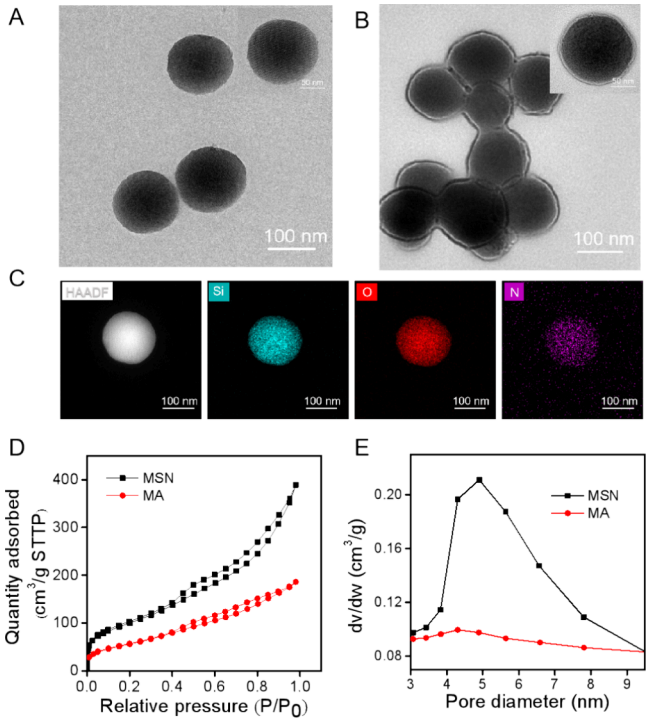

Figure 2. TEM images of (A) MSN and (B) MA. (C) Elemental mapping analysis of MA nanoparticles. (D) Nitrogen adsorption−desorption curves of MSN and MA, respectively. (E) Pore size distribution curves of MSN and MA, respectively.

surface of MSN. In essence, the surface of MSN is grafted with a boric acid structure, which then undergoes a complexation reaction with the o-hydroxyl group of HA. This dynamic cross-linking bond effectively fixes HA onto the MSN surface, leading to the formation of aggregates.[50] The N_2 adsorption−desorption isotherms of MSNs corresponded to typical type IV, demonstrating the mesoporous structure of these products (Figure 2D). In addition, the specific surface area of MA (368.5 cm^3/g) was slightly different from that of MSNs (429.5 cm^3/g). When the surface of MSNs is modified with HA, the size of the nanoparticles increases, consequently leading to a reduction in the corresponding specific surface area. Meanwhile, the pore size of MSNs was 4.8 nm, while the pore volume of the MSNs was significantly reduced. These results indicated that HA was successfully coated onto MSNs (Figure 2D,E).

The MA aims to achieve targeted and stimuli-responsive drug release for cancer therapy. To demonstrate this potential, DOX was chosen as the model molecule to develop MSN-NH_2−CPBA-HA@DOX (MAD). The DLS measurements determined that the mean hydrodynamic diameters of MSNs and MA were 210.2 ± 21.9 and 240.9 ± 23.3 nm, respectively (Figure 3A). Upon loading DOX, MAD showed a slight increase in diameter (252.9 ± 24.3) (Figure 3A), indicating that the presence of this hydrophilic drug induces a slight alteration in the size of the nanomedicine carrier and improves the polydispersity of MSN. Moreover, MSNs exhibited a negative surface potential of −10.8 ± 1.3 mV. After HA packaging, the surface potential of MA was observed to be −15.6 ± 1.8 mV (Figure 3B). The surface potential of MAD was lower than that of MA (Figure 3B), likely due to the positively charged DOX loaded into MA. The HA plays a crucial role in forming a negatively charged polymer layer on

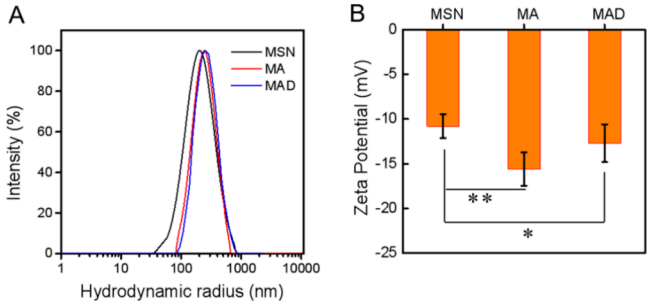

Figure 3. Hydrodynamic size (A) and Zeta potential (B) of MSN, MA, and MAD nanoparticles.

the surface of MSNs. This layer imparts a negative surface charge to the entire MSNs, facilitating the adsorption of positively charged DOX. As a result, when DOX is loaded onto the MSNs, the negative surface charge of the MSN-DOX complex is slightly reduced.

To further confirm the successful preparation of MAD, different samples were compared by using TGA, FTIR, and UV−vis spectroscopy. Thermogravimetric analysis revealed a weight loss of up to 20% in the MAD group (Figure 4A,B),

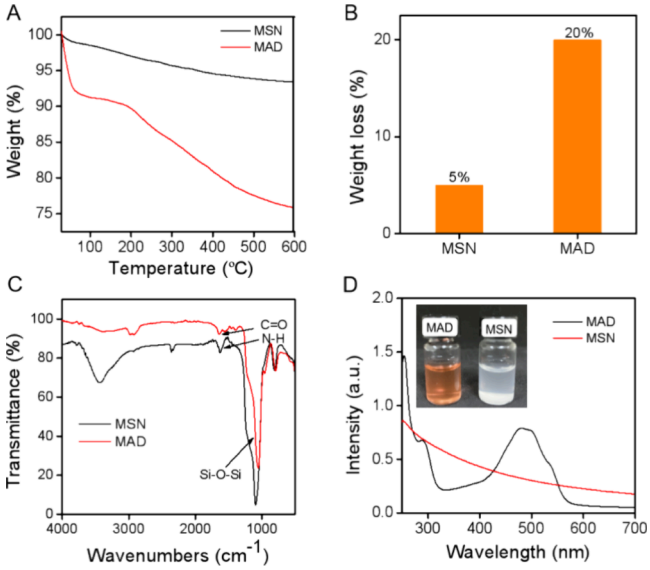

Figure 4. (A) Thermogravimetric analysis of the MSN and MAD. (B) Quantitative data from thermogravimetric analysis. (C) FTIR spectra of MSN and MAD. (D) UV−vis spectra of MSN and MAD. The photo on the upper left corner in (D) shows MAD and MSN after they were placed in PBS solution for 48 h.

which may be attributed to the loss of HA and DOX. The FTIR spectra of MAD showed three characteristic peaks at 1100, 800, and 1540 cm^{-1} (Figure 4C). The first two peaks were consistent with those in the spectra of MSNs, representing antisymmetric and symmetric Si−O−Si stretching vibrations. The new peak at 1540 cm^{-1} suggested that amine groups were immobilized on the surface of the MSNs. Furthermore, the amide bond peaks appeared near 1550 and 1645 cm^{-1}, indicating that HA successfully covered the MSNs. In the UV−vis spectrum of MAD, a characteristic peak was observed at 490 nm (Figure 4D), corresponding to the wavelength of DOX, which revealed the successful entrapment of DOX. Moreover, MAD and MSNs were dispersed in a PBS

https://doi.org/10.1021/acsomega.4c04502
ACS Omega 2024, 9, 47428−47435

solution for 48 h. During this period, sedimentation occurred in the MSNs group, whereas the MAD group remained as a transparent red solution. The MAD showed good colloidal stability in PBS solutions at different pHs even after 5 days (Figure S1). This finding indicated that the modified MSNs are more suitable for body fluid circulation, thereby enhancing their capability to exert antitumor effects.

3.2. Drug Loading Capacity and Multistimuli Responsive Drug Release of the Nanohybrid. The effective therapeutic outcomes of nanomedicine significantly rely on its efficient loading capacity and controlled release mechanisms. Specifically, the controlled release of drugs in response to various tumor microenvironment characteristics plays a pivotal role in enhancing the treatment efficacy. To demonstrate this, a comparison of the loading capacity of MSN for DOX before and after modification was conducted. The results showed that unmodified MSN exhibited a loading efficiency of 45.7% ± 2.6% for DOX, whereas modification with HA increased this efficiency to 75.3% ± 3.7% (Figure 5A). The results of loading DOX and MA at varying concentrations demonstrated that different concentrations of DOX had little effect on the size of the MAD (Figure S2). This enhancement in loading capacity with modification suggests that the presence of HA on MSN effectively increases the adsorption potential of hybrid nanoparticles for DOX, likely due to the increased number of adsorption sites and the network structure offered by the modification. Moreover, in a comparative release study where free DOX and MAD were concurrently exposed to PBS solution, rapid filtration of DOX was observed within 4 h, whereas MAD exhibited sustained release for up to 48 h (Figure 5B). This sustained release capability of MAD indicates its distinct slow-release effect on DOX, offering promising implications for controlled drug delivery strategies in cancer therapy.

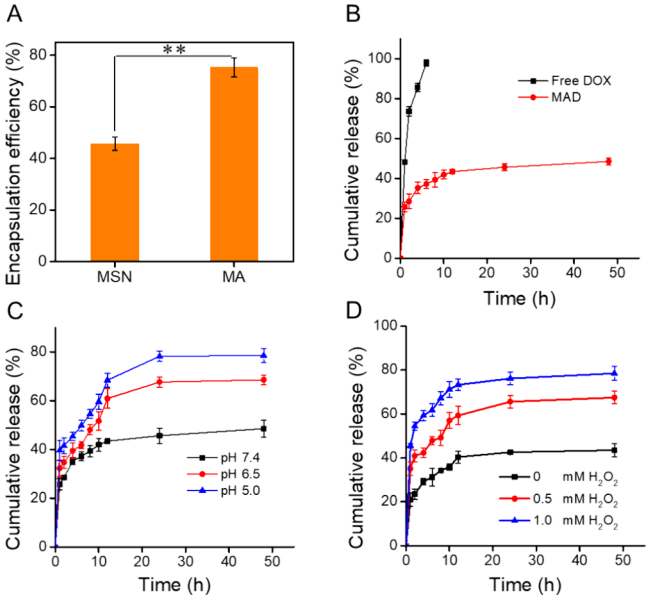

Figure 5. Drug loading and stimuli-responsive release properties. (A) Drug encapsulation efficiency of MSN and MA. (B) DOX release curves of free DOX and MAD in PBS buffer at pH 7.4 and 37 °C. (C) DOX release curve from MAD at pH values of 5.0, 6.5, and 7.4. (D) DOX release curve from MAD in different concentrations of H_2O_2 (0, 0.5, and 1.0 mM).

The excessive proliferation of tumor cells leads to a weakly acidic microenvironment, which is a crucial factor influencing the drug release of nanohybrids.[51] To further examine the drug release behavior, MAD was placed in PBS solutions with varying pH values. The results revealed significant differences in the drug release patterns of MAD under different pH conditions. Specifically, at pH 5.0, MAD achieved a cumulative drug release efficiency of 80% within a 48 h period. This notable release profile could be attributed to the presence of a responsive borate structure in MAD, facilitating pH-responsive drug release (Figure 5C). Furthermore, studies have indicated an abundance of ROS in the tumor microenvironment, which can trigger the cleavage of the borate structure. The results indicated that MAD could effectively release DOX in response to varying concentrations of H_2O_2, with the cumulative drug release efficiency reaching 78.5% at a concentration of 1.0 mM H_2O_2 (Figure 5D). In conclusion, this controlled drug release system leverages the responsiveness of the borate bond to ensure that the drug is released entirely at the desired location and optimal time, potentially enhancing therapeutic effects while minimizing side effects. The ability to tune the release rate based on environmental conditions makes this approach highly desirable for targeted drug delivery.

3.3. In Vitro Cytocompatibility. The biocompatibility of nanodrug carriers plays a pivotal role in their in vivo application.[52] In a previous report, the coculture of MSN and MA with L929 cells revealed distinct green fluorescence with minimal red fluorescence, indicating that MSN and MA had a negligible effect on the growth of L929 cells (Figure 6A). Moreover, when exposed to varying concentrations of MSN, MA, and MAD, L929 cells maintained a survival rate exceeding 80% even at 400 μg/mL, indicating the substantial biocompatibility of the nanomaterials. Notably, the survival

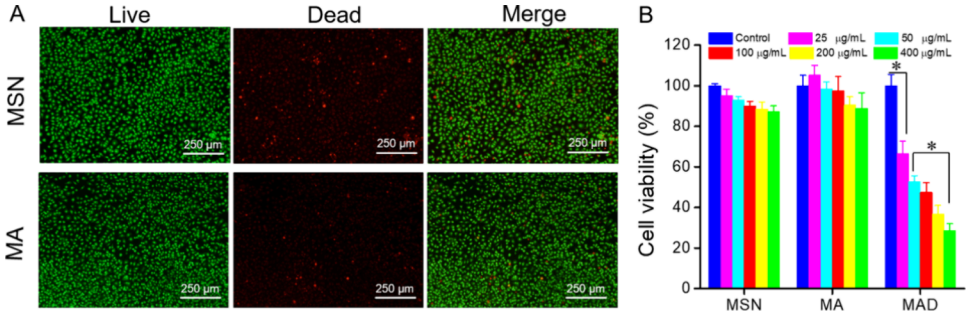

Figure 6. In vitro biocompatibility of MSN, MA, and MAD. (A) Live/dead staining images of L929 cells incubated with MSN and MA (200 μg/mL). (B) Cell viability of L929 cells incubated with different concentrations of MSN, MA, and MAD. (±standard deviation, $n = 3$; * $P < 0.05$).

https://doi.org/10.1021/acsomega.4c04502
ACS Omega 2024, 9, 47428−47435

rate of cells in the MA group was higher than that in the MSN group at equivalent concentrations (Figure 6B). This finding indicates that HA modification can enhance the biocompatibility of MSN, thereby increasing its potential for biological applications. Moreover, the results demonstrated that the cytotoxic effect of MAD on A549 cells was significantly superior to that on L929 cells at the same concentration. This difference in efficacy can be ascribed to the presence of the CD44 receptor and the overexpression of hyaluronidase in A549 cells.[53]

3.4. In Vitro Cytotoxicity and Uptake of MAD. The MA exhibited an effective loading and sustained release of DOX, signifying its potential for targeted cancer therapy. The cytotoxicity of MAD toward cancer cells was subsequently evaluated. When the DOX concentration was below 1 μM, free DOX exhibited slight cytotoxicity against cancer cells, with more than 75% of the cells remaining viable. Notably, cancer cell survival decreased to 52.8% in the presence of MAD, indicating an enhanced cellular uptake efficiency. Furthermore, as the DOX concentration increased, MAD exhibited markedly superior cytotoxicity compared to that of the free DOX group. The IC50 values of DOX and MAD were recorded at 2.48 and 1.12 μM, respectively (Figure 7B). We further evaluated the therapeutic efficacy of nanoparticles by analyzing their uptake in cancer cells, specifically observing the distribution of DOX (indicated by red fluorescence) within the cells using confocal laser scanning microscopy (Figure 7C). After treatment for 4 h, cells treated with MAD exhibited obvious red fluorescence, while the control group showed minimal to no red fluorescence, suggesting that MAD was rapidly taken up by A549 cells. Moreover, after treatment for 24 h, the MAD group exhibited more intense red fluorescence compared to the DOX group, and the fluorescence intensity of MAD was 2.5 times that of DOX (Figure S3). Free DOX primarily enters cells via passive diffusion, a relatively limited mechanism of cellular uptake, resulting in a weaker fluorescence intensity within 24 h. Studies have shown that HA has a strong affinity for cancer cells, thereby enhancing the uptake of MAD by these cells. MSN as a traditional drug carrier in tumor treatment has gained significant attention. Its unique properties and versatile nature have made it an invaluable tool in the battle against cancer. However, a major hurdle in its application has been the issue of unstable drug release. In contrast, MA exhibits superior tumor cell targeting capabilities along with enhanced drug loading efficiency. Furthermore, MA possesses the capability to release drugs specifically to eliminate tumor cells upon stimulation from the tumor microenvironment. Hence, MAD holds significant promise as a potential cancer treatment.

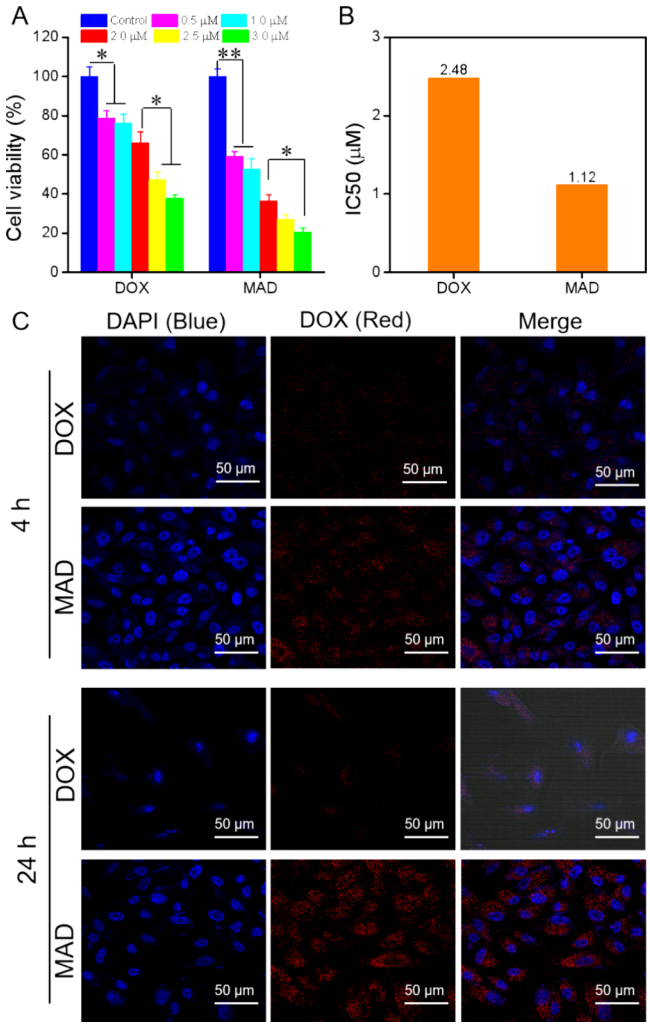

Figure 7. In vitro cytotoxicity of MAD. (A) Cell viability of A549 cells incubated with different concentrations of DOX and MAD (with the equivalent DOX concentration) for 48 h. (B) IC50 values for A549 cells. (C) Confocal laser scanning microscopy images of DOX and MAD cocultured with A549 cells for 4 and 24 h (±standard deviation, $n = 3$; $^{*}P < 0.05$, $^{**}P < 0.01$).

4. CONCLUSIONS

To enhance antitumor efficacy, a novel strategy was employed to fabricate an MSN-based nanoplatform (MAD) with robust stability and targeting capabilities. The MAD comprises four components: CPBA-functionalized MSN, HA immobilized on the MSN surface, a stimuli-responsive PBAE bond connecting CPBA-MSN and HA, and the chemotherapeutic agent DOX. The MAD demonstrated a high DOX encapsulation efficiency of 75%. Dispersion and uptake tests revealed that HA conferred favorable stability and enhanced interactions with cancer cells. The DOX release profiles indicated that MAD was sensitive to acidic conditions and ROS, enabling tumor-specific drug release. Taken together, MAD exhibited safe and efficient antitumor activity, presenting a promising approach for targeted drug delivery.

■ ASSOCIATED CONTENT

Supporting Information

The Supporting Information is available free of charge at https://pubs.acs.org/doi/10.1021/acsomega.4c04502.

Zeta potential changes of MAD at different pH values within 5 days, drug encapsulation efficiency of DOX at different concentrations and hydrodynamic size of MAD, and the quantitative DOX fluorescence intensity of A549 cells (PDF)

■ AUTHOR INFORMATION

Corresponding Author

Zhe Liu − *School of Stomatology, Jiangxi Medical College, Nanchang University, Nanchang 330006, China; Jiangxi Province Key Laboratory of Oral Biomedicine, Nanchang 330006, China; Jiangxi Province Clinical Research Center for*

https://doi.org/10.1021/acsomega.4c04502
ACS Omega 2024, 9, 47428−47435

Oral Diseases, Nanchang 330006, China; orcid.org/0009-0000-3310-4736; Email: Liuzhepang88@163.com

Authors

Yurong Leng − *School of Stomatology, Jiangxi Medical College, Nanchang University, Nanchang 330006, China; Jiangxi Province Key Laboratory of Oral Biomedicine, Nanchang 330006, China; Jiangxi Province Clinical Research Center for Oral Diseases, Nanchang 330006, China*

Yanmei Wu − *School of Stomatology, Jiangxi Medical College, Nanchang University, Nanchang 330006, China; Jiangxi Province Key Laboratory of Oral Biomedicine, Nanchang 330006, China; Jiangxi Province Clinical Research Center for Oral Diseases, Nanchang 330006, China*

Wenjing Xiao − *School of Stomatology, Jiangxi Medical College, Nanchang University, Nanchang 330006, China*

Xiaoquan Su − *School of Stomatology, Jiangxi Medical College, Nanchang University, Nanchang 330006, China*

Complete contact information is available at: https://pubs.acs.org/10.1021/acsomega.4c04502

Notes

The authors declare no competing financial interest.

■ ACKNOWLEDGMENTS

Not available.

■ REFERENCES

(1) Grodzinski, P.; Kircher, M.; Goldberg, M.; Gabizon, A. Integrating nanotechnology into cancer care. *ACS Nano* **2019**, *13* (7), 7370−7376.

(2) Kanwar, R.; Rathee, J.; Salunke, D. B.; Mehta, S. K. Green nanotechnology-driven drug delivery assemblies. *ACS omega* **2019**, *4* (5), 8804−8815.

(3) Perry, J. L.; Reuter, K. G.; Luft, J. C.; Pecot, C. V.; Zamboni, W.; DeSimone, J. M. Mediating passive tumor accumulation through particle size, tumor type, and location. *Nano Lett.* **2017**, *17* (5), 2879−2886.

(4) Teixeira, P. V.; Fernandes, E.; Soares, T. B.; Adega, F.; Lopes, C. M.; Lúcio, M. Natural compounds: co-delivery strategies with chemotherapeutic agents or nucleic acids using lipid-based nanocarriers. *Pharmaceutics* **2023**, *15* (4), 1317.

(5) Pandit, G.; Roy, K.; Agarwal, U.; Chatterjee, S. Self-assembly mechanism of a peptide-based drug delivery vehicle. *ACS omega* **2018**, *3* (3), 3143−3155.

(6) Chen, M.; Bhattarai, N.; Cong, M.; Pérez, R. L.; McDonough, K. C.; Warner, I. M. Mitochondria targeting IR780-based nano-GUMBOS for enhanced selective toxicity towards cancer cells. *RSC Adv.* **2018**, *8* (55), 31700−31709.

(7) Li, C.; Wang, J.; Wang, Y.; Gao, H.; Wei, G.; Huang, Y.; Yu, H.; Gan, Y.; Wang, Y.; Mei, L.; et al. Recent progress in drug delivery. *Acta Pharm. Sin. B* **2019**, *9* (6), 1145−1162.

(8) Zhu, W.; Huang, W.; Ye, L.; Deng, Y.; Xie, Q.; Jiang, Y. Facile preparation of succinylated-zein-ZIF-8 hybrid for enhanced stability and pH-responsive drug delivery. *Chem. Eng. Sci.* **2020**, *228*, No. 115981.

(9) Leonetti, B.; Perin, A.; Ambrosi, E. K.; Sponchia, G.; Sgarbossa, P.; Castellin, A.; Riello, P.; Scarso, A. Mesoporous zirconia nanoparticles as drug delivery systems: drug loading, stability and release. *J. Drug Delivery Sci. Tec.* **2021**, *61*, No. 102189.

(10) Sainaga Jyothi, V. G. S.; Bulusu, R.; Venkata Krishna Rao, B.; Pranothi, M.; Banda, S.; Kumar Bolla, P.; Kommineni, N. Stability characterization for pharmaceutical liposome product development with focus on regulatory considerations: An update. *Int. J. Pharm.* **2022**, *624*, No. 122022.

(11) Yin, Y.; Guan, L.; Wang, Y.; Ma, Y.; Pan, J.; Peng, Y.; Pan, G. Sialic acid-imprinted mesoporous nanocarriers for tumor cell targeted drug delivery. *Colloid Interface Sci.* **2021**, *42*, No. 100421.

(12) Tian, Y.; Tian, R.; Chen, L.; Jin, R.; Feng, Y.; Bai, Y.; Chen, X. Redox-responsive nanogel with intracellular reconstruction and programmable drug release for targeted tumor therapy. *Macromol. Rapid Commun.* **2019**, *40* (8), No. 1800824.

(13) Pallares, R. M.; Abergel, R. J. Nanoparticles for targeted cancer radiotherapy. *Nano Res.* **2020**, *13* (11), 2887−2897.

(14) Zhao, N.; Yan, L.; Zhao, X.; Chen, X.; Li, A.; Zheng, D.; Zhou, X.; Dai, X.; Xu, F.-J. Versatile types of organic/inorganic nanohybrids: from strategic design to biomedical applications. *Chem. Rev.* **2019**, *119* (3), 1666−1762.

(15) Yañez-Aulestia, A.; Gupta, N. K.; Hernández, M.; Osorio-Toribio, G.; Sánchez-González, E.; Guzmán-Vargas, A.; Rivera, J. L.; Ibarra, I. A.; Lima, E. Gold nanoparticles: current and upcoming biomedical applications in sensing, drug, and gene delivery. *Chem. Commun.* **2022**, *58* (78), 10886−10895.

(16) Qiao, R.; Fu, C.; Forgham, H.; Javed, I.; Huang, X.; Zhu, J.; Whittaker, A. K.; Davis, T. P. Magnetic iron oxide nanoparticles for brain imaging and drug delivery. *Adv. Drug Deliver. Rev.* **2023**, *197*, No. 114822.

(17) Ahmed, H.; Gomte, S. S.; Prathyusha, E.; A, P.; Agrawal, M.; Alexander, A. Biomedical applications of mesoporous silica nanoparticles as a drug delivery carrier. *J. Drug Delivery Sci. Tec.* **2022**, *76*, No. 103729.

(18) Xin, J.; Lu, X.; Cao, J.; Wu, W.; Liu, Q.; Wang, D.; Zhou, X.; Ding, D. Fluorinated organic polymers for cancer drug delivery. *Adv. Mater.* **2024**, *36*, No. 2404645. (acccessed 2024/05/08).

(19) Zhang, Y.; Sun, T.; Jiang, C. Biomacromolecules as carriers in drug delivery and tissue engineering. *Acta Pharm. Sin. B* **2018**, *8* (1), 34−50.

(20) Iturrioz-Rodríguez, N.; Correa-Duarte, M. A.; Fanarraga, M. L. Controlled drug delivery systems for cancer based on mesoporous silica nanoparticles. *Int. J. Nanomed.* **2019**, *14*, 3389−3401.

(21) Seljak, K. B.; Kocbek, P.; Gašperlin, M. Mesoporous silica nanoparticles as delivery carriers: An overview of drug loading techniques. *J. Drug Delivery Sci. Tec.* **2020**, *59*, No. 101906.

(22) Huang, L.; Liu, J.; Gao, F.; Cheng, Q.; Lu, B.; Zheng, H.; Xu, H.; Xu, P.; Zhang, X.; Zeng, X. A dual-responsive, hyaluronic acid targeted drug delivery system based on hollow mesoporous silica nanoparticles for cancer therapy. *J. Mater. Chem. B* **2018**, *6* (28), 4618−4629.

(23) Cui, L.; Liu, W.; Liu, H.; Qin, Q.; Wu, S.; He, S.; Pang, X.; Zhu, C.; Shen, P. pH-Triggered charge-reversal mesoporous silica nanoparticles stabilized by chitosan oligosaccharide/carboxymethyl chitosan hybrids for effective intracellular delivery of doxorubicin. *ACS Appli. Bio Mater.* **2019**, *2* (5), 1907−1919.

(24) Luo, W.; Xu, X.; Zhou, B.; He, P.; Li, Y.; Liu, C. Formation of enzymatic/redox-switching nanogates on mesoporous silica nanoparticles for anticancer drug delivery. *Mater. Sci. Eng., C* **2019**, *100*, 855−861.

(25) Du, J.; Wang, L.; Han, X.; Dou, J.; Jiang, X.; Yuan, J. Polydopamine/keratin complexes as gatekeepers of mesoporous silica nanoparticles for pH and GSH dual responsive drug delivery. *Mater. Lett.* **2021**, *293*, No. 129676.

(26) Enyu, X.; Liu, L.; Chen, X.; Chen, H.; Chen, Y.; Chen, Y. Construction and performance evaluation of pH-responsive oxidized hyaluronic acid hollow mesoporous silica nanoparticles. *Int. J. Biol. Macromol.* **2024**, *257*, No. 128656.

(27) Zhang, J.; Sun, Y.; Tian, B.; Li, K.; Wang, L.; Liang, Y.; Han, J. Multifunctional mesoporous silica nanoparticles modified with tumor-shedable hyaluronic acid as carriers for doxorubicin. *Colloid. Surface. B* **2016**, *144*, 293−302.

(28) Lu, J.; Luo, B.; Chen, Z.; Yuan, Y.; Kuang, Y.; Wan, L.; Yao, L.; Chen, X.; Jiang, B.; Liu, J. Host-guest fabrication of dual-responsive hyaluronic acid/mesoporous silica nanoparticle based drug delivery system for targeted cancer therapy. *Int. J. Biol. Macromol.* **2020**, *146*, 363−373.

(29) Palanikumar, L.; Kim, J.; Oh, J. Y.; Choi, H.; Park, M.; Kim, C.; Ryu, J. Hyaluronic acid-modified polymeric gatekeepers on biodegradable mesoporous silica nanoparticles for targeted cancer therapy. *ACS Biomater. Sci. Eng.* **2018**, *4* (5), 1716−1722.
(30) Song, Y.; Li, Y.; Xu, Q.; Liu, Z. Mesoporous silica nanoparticles for stimuli-responsive controlled drug delivery: advances, challenges, and outlook. *Int. J. Nanomed.* **2017**, *12*, 87−110.
(31) Watermann, A.; Brieger, J. Mesoporous silica nanoparticles as drug delivery vehicles in cancer. *Nanomaterials* **2017**, *7* (7), 189.
(32) Bahrami, F.; Abdekhodaie, M. J.; Behroozi, F.; Mehrvar, M. Nano mesoporous silica for cancer treatment: ROS-responsive and redox-responsive carriers. *J. Drug Delivery Sci. Tec.* **2020**, *57*, No. 101510.
(33) Chen, X.; Liu, Z. Dual responsive mesoporous silica nanoparticles for targeted co-delivery of hydrophobic and hydrophilic anticancer drugs to tumor cells. *J. Mater. Chem. B* **2016**, *4* (25), 4382−4388.
(34) Zhao, Q.; Wang, S.; Yang, Y.; Li, X.; Di, D.; Zhang, C.; Jiang, T.; Wang, S. Hyaluronic acid and carbon dots-gated hollow mesoporous silica for redox and enzyme-triggered targeted drug delivery and bioimaging. *Mater. Sci. Eng., C* **2017**, *78*, 475−484.
(35) Hossen, S.; Hossain, M. K.; Basher, M. K.; Mia, M. N. H.; Rahman, M. T.; Uddin, M. J. Smart nanocarrier-based drug delivery systems for cancer therapy and toxicity studies: A review. *J. Adv. Res.* **2019**, *15*, 1−18.
(36) Ding, X.; Yu, W.; Wan, Y.; Yang, M.; Hua, C.; Peng, N.; Liu, Y. A pH/ROS-responsive, tumor-targeted drug delivery system based on carboxymethyl chitin gated hollow mesoporous silica nanoparticles for anti-tumor chemotherapy. *Carbohyd. Polym.* **2020**, *245*, No. 116493.
(37) N, V. R.; Han, H. S.; Lee, H.; Nguyen, V. Q.; Jeon, S.; Jung, D.-W.; Lee, J.; Yi, G.-R.; Park, J. H. ROS-responsive mesoporous silica nanoparticles for MR imaging-guided photodynamically maneuvered chemotherapy. *Nanoscale* **2018**, *10* (20), 9616−9627.
(38) Daund, V.; Chalke, S.; Sherje, A. P.; Kale, P. P. ROS responsive mesoporous silica nanoparticles for smart drug delivery: A review. *J. Drug Delivery Sci. Tec.* **2021**, *64*, No. 102599.
(39) He, Q.; Chen, J.; Yan, J.; Cai, S.; Xiong, H.; Liu, Y.; Peng, D.; Mo, M.; Liu, Z. Tumor microenvironment responsive drug delivery systems. *Asian J. Pharm. Sci.* **2020**, *15* (4), 416−448.
(40) Chen, W.; Xie, W.; Zhao, G.; Shuai, Q. Efficient pH-responsive nano-drug delivery system based on dynamic boronic acid/ester transformation. *Molecules* **2023**, *28* (11), 4461.
(41) Wang, H.; Wang, L.; Guo, S.; Liu, Z.; Zhao, L.; Qiao, R.; Li, C. Rutin-Loaded Stimuli-Responsive Hydrogel for Anti-Inflammation. *ACS Appli. Mater. Interfaces* **2022**, *14* (23), 26327−26337.
(42) Sarkar, S.; Sadhukhan, P.; Das, D.; Basyach, P.; Das, J.; Das, M.; Saikia, L.; Wann, S.; Kalita, J.; Sil, P.; Manna, P. Glucose-sensitive delivery of vitamin k by using surface-functionalized, dextran-capped mesoporous silica nanoparticles to alleviate hyperglycemia. *ACS Appl. Mater. Interfaces* **2022**, *14* (23), 26489−26500.
(43) Hou, L.; Zheng, Y.; Wang, Y.; Hu, Y.; Shi, J.; Liu, Q.; Zhang, H.; Zhang, Z. Self-regulated carboxyphenylboronic acid-modified mesoporous silica nanoparticles with "touch switch" releasing property for insulin delivery. *ACS Appl. Mater. Interfaces* **2018**, *10* (26), 21927−21938.
(44) Zhou, D.; Liu, S.; Hu, Y.; Yang, S.; Zhao, B.; Zheng, K.; Zhang, Y.; He, P.; Mo, G.; Li, Y. Tumor-mediated shape-transformable nanogels with pH/redox/enzymatic-sensitivity for anticancer therapy. *J. Mater. Chem. B* **2020**, *8* (17), 3801−3813.
(45) Li, K.; Zhou, D.; Cui, H.; Mo, G.; Liu, Y.; Zheng, Z.; Li, J.; Ping, D.; Sun, J.; Zhang, Y.; Gao, J. Size-transformable gelatin/nanochitosan/doxorubicin nanoparticles with sequentially triggered drug release for anticancer therapy. *Colloids Surf., B* **2022**, *220*, No. 112927.
(46) Pham, X.; Tran, V. K.; Hahm, E.; Kim, Y.; Kim, J.; Kim, W.; Jun, B. Synthesis of gold-platinum core-shell nanoparticles assembled on a silica template and their peroxidase nanozyme properties. *Int. J. Mol. Sci.* **2022**, *23* (12), 6424.
(47) Dong, H.; Ma, Y.; Li, R.; Zhang, W.; Zhang, M.; Meng, F.; Ding, K.; Jiang, H.; Gong, Y. Smart MSN-drug-delivery system for tumor cell targeting and tumor microenvironment release. *ACS Appl. Mater. Interfaces* **2021**, *13* (36), 42522−42532.
(48) Ugur, N.; Harputlu, E.; Sezer, C.; Demirdogen, R.; Ince, M.; Unlu, G.; Yurt, F.; Emen, F.; Kutlu, H.; Ocakoglu, K. Investigation of in vitro biological activities of hollow mesoporous carbon nanoparticles bearing D-NMAPPD on human lung adenocarcinoma cells. *J. Drug Delivery Sci. Tec.* **2022**, *67*, No. 102778.
(49) Pushpalatha, R.; Selvamuthukumar, S.; Kilimozhi, D. Nanocarrier mediated combination drug delivery for chemotherapy−A review. *J. Drug Delivery Sci. Tec.* **2017**, *39*, 362−371.
(50) Shi, W.; Hass, B.; Kuss, M. A.; Zhang, H.; Ryu, S.; Zhang, D.; Li, T.; Li, Y.; Duan, B. Fabrication of versatile dynamic hyaluronic acid-based hydrogels. *Carbohyd. polym.* **2020**, *233*, No. 115803.
(51) Deirram, N.; Zhang, C.; Kermaniyan, S. S.; Johnston, A. P.; Such, G. K. pH-responsive polymer nanoparticles for drug delivery. *Macromol. rapid com.* **2019**, *40* (10), No. 1800917.
(52) Li, Z.; Zhang, Y.; Feng, N. Mesoporous silica nanoparticles: synthesis, classification, drug loading, pharmacokinetics, biocompatibility, and application in drug delivery. *Expert Opin. Drug Del.* **2019**, *16* (3), 219−237.
(53) Seo, J.; Lee, S.; Hwang, C.; Yang, M.; Lee, J. M.; Lee, S. H.; Cho, H. Multi-layered cellulose nanocrystal system for CD44 receptor-positive tumor-targeted anticancer drug delivery. *Int. J. Biol. Macromol.* **2020**, *162*, 798−809.

https://doi.org/10.1021/acsomega.4c04502
ACS Omega 2024, 9, 47428−47435